The full potential Korringa–Kohn–Rostoker method and its application in electric field gradient calculations

2005 J. Phys.: Condens. Matter 17 5741

(http://iopscience.iop.org/0953-8984/17/37/011)

INSTITUTE OF PHYSICS PUBLISHING JOURNAL OF PHYSICS: CONDENSED MATTER

J. Phys.: Condens. Matter **17** (2005) 5741–5755 doi:10.1088/0953-8984/17/37/011

The full potential Korringa–Kohn–Rostoker method and its application in electric field gradient calculations

M Ogura and H Akai

Department of Physics, Graduate School of Science, Osaka University, 1-1 Machikaneyama, Toyonaka, Osaka 560-0043, Japan

Received 13 May 2005, in final form 11 August 2005
Published 2 September 2005
Online at stacks.iop.org/JPhysCM/17/5741

Abstract

We have developed a full potential Korringa–Kohn–Rostoker (KKR) Green function method. Three improvements which make the full potential treatment efficient and practical are reported. One is a method for constructing the Green function which satisfies the Wronskian relation exactly. The second is including the contribution of the non-spherical part of the potential in the wavefunctions correctly by use of a modified recursive integral equation. Thirdly, we propose a method that completely eliminates the contribution of irregular solutions of the Schrödinger equation to charge/spin densities. In order to check the reliability of the method, we calculated the electric field gradient (EFG), which is sensitive to how the potential is treated. We have performed EFG calculations for hcp metals and sp impurities in Zn and Cd with the present method. The results are in good agreement with experimental data and show that the full potential KKR method is reliable enough for EFG calculations.

1. Introduction

The electric field gradient (EFG) is an important clue to the local electronic behaviour of solids. Using the information obtained through EFG measurements, together with theoretical analyses of the electronic structure of the system, one can determine the local electronic behaviour as well as the geometry of the lattice around the probe nuclei rather precisely. Such an approach has become more important due to the development of experimental techniques such as the nuclear magnetic resonance (NMR), β-NMR, perturbed angular correlation (PAC) and Mössbauer spectroscopy approaches, which make it possible to determine EFGs in very complex systems. However, in order to make the theoretical analyses meaningful for these complex systems, one first of all needs a highly reliable description of the anisotropy of the electron density distributions. For this reason, improvement of the theoretical method for describing the electronic structure is crucial. The purpose of the present study is to develop a

full potential method, which is necessary to give a reliable description of the anisotropy of the electron distribution, in the framework of the KKR Green function method.

Theoretical analyses of EFGs have been so far been made mainly on the basis of self-consistent electronic structure calculations using the full potential linearized augmented plane wave (FLAPW) method. In the FLAPW method, the wavefunctions are expanded into atomic-like functions inside non-overlapping muffin-tin spheres around the atoms and into plane waves in the interstitial region. The charge density and the potential are written as a linear combination of radial functions times symmetrized lattice harmonics inside the spheres and as a Fourier series in the interstitial region [1]. Thus no shape approximations are made for the description of the potential. This procedure is frequently called the *full potential* approach. It is important for the EFG calculation. In contrast to the sophisticated way of constructing the potential, the FLAPW method generates atomic-like radial functions, which are used as a variational basis set, using only the spherical part of the potential inside the sphere. In other words, the full potential is not used for generating the wavefunctions inside the sphere, meaning that they are not fully self-consistent.

Recently, several groups have tried to develop a full potential scheme which uses the full potential not only in the restricted sense, as in FLAPW approach, but also in generating the wavefunctions. An extension of the Korringa–Kohn–Rostoker (KKR) Green function method is one such attempt. The KKR method has many advantages such as high speed, high precision and applicability to a large class of problems requiring the use of Green functions, including the impurity problems, disordered systems treated by the coherent potential approximation (CPA) [2, 3], transport properties and many-body perturbation theories. Drittler *et al* were the first to develop the full potential KKR method [4, 5]. Their method took account of the non-spherical parts of the potential in generating the wavefunctions in the sense of the Born series. Hence, it could exactly treat the full potential. They applied the method in an EFG calculation for dilute Cu alloys successfully and showed that the dominant contribution was the Cu d electrons [4]. From the practical point of view, however, the method is not yet fully satisfactory for electronic structure calculations for arbitrary solids. This is mainly because of the complicated analytical properties of the full potential KKR method.

We have independently developed a full potential KKR method. Though our method is mostly based on the formalism given by Drittler, it has some new features that were missing in the latter. These new features solve most of the difficulties arising in the full potential KKR method, considerably enhance the power of the method and also improve the numerical stability and precision as well as the computational speed. We explain these points in section 2 and give the results of the EFG calculations for hcp metals made using the full potential KKR method in section 3. We compare them with the FLAPW results and experimental data, and the influence of the description of the potential for EFGs is investigated. In addition, the relativistic effects on the EFG are discussed. We also show the results of the EFG calculations for impurities in Zn and Cd.

2. Full potential KKR Green function method

2.1. Basic idea

In the full potential KKR, the crystal is divided into Voronoi cells which define a non-overlapping cell potential $V^n(\boldsymbol{r})$ in each cell. For such cell potentials the cell-centred Green function is expanded as [6]

$$G(\boldsymbol{r}+\boldsymbol{R}^n, \boldsymbol{r}'+\boldsymbol{R}^{n'}; E) = \delta_{nn'} G^n_s(\boldsymbol{r}, \boldsymbol{r}'; E) + \sum_L R^n_L(\boldsymbol{r}; E) \sum_{L'} G^{nn'}_{LL'}(E) R^{n'}_{L'}(\boldsymbol{r}'; E) \qquad (1)$$

where $\boldsymbol{R}^n$ denotes the centre of the nth Voronoi cell, L denotes a set of the orbital angular momentum l and the magnetic quantum number m, and $G_s^n(\boldsymbol{r}, \boldsymbol{r}'; E)$ is the single-site Green function defined by

$$G_s^n(\boldsymbol{r}, \boldsymbol{r}'; E) = \sqrt{E} \sum_L R_L^n(\boldsymbol{r}_<; E) H_L^n(\boldsymbol{r}_>; E). \tag{2}$$

$R_L^n(\boldsymbol{r}; E)$ and $H_L^n(\boldsymbol{r}; E)$ are the regular and irregular solutions of the single-site Schrödinger equation, respectively:

$$\left[-\nabla^2 + V^n(\boldsymbol{r})\right] R_L^n(\boldsymbol{r}; E) = E R_L^n(\boldsymbol{r}; E) \tag{3}$$

$$\left[-\nabla^2 + V^n(\boldsymbol{r})\right] H_L^n(\boldsymbol{r}; E) = E H_L^n(\boldsymbol{r}; E) \tag{4}$$

and $\boldsymbol{r}_<$ ($\boldsymbol{r}_>$) is the smaller (larger) of $\boldsymbol{r}$ and $\boldsymbol{r}'$. The boundary conditions for $R_L^n(\boldsymbol{r}; E)$ and $H_L^n(\boldsymbol{r}; E)$ will be given later in equations (19) and (20). The structural Green function $G_{LL'}^{nn'}(E)$ satisfies the following Dyson-type equation:

$$G_{LL'}^{nn'}(E) = g_{LL'}^{nn'}(E) + \sum_{L''n''} g_{LL''}^{nn''}(E) \sum_{L'''} t_{L''L'''}^{n''}(E) G_{L'''L'}^{n''n}(E), \tag{5}$$

with the free space structure constant $g_{LL'}^{nn'}(E)$ [7] and the t-matrix $t_{LL'}^n(E)$ for each cell potential. The t-matrix is defined by

$$t_{LL'}^n(E) = \int \mathrm{d}\boldsymbol{r}\, j_l(\sqrt{E}r) Y_L(\hat{\boldsymbol{r}}; E) V^n(\boldsymbol{r}) R_{L'}^n(\boldsymbol{r}; E), \tag{6}$$

where $j_l(z)$ is the spherical Bessel function.

Next, we outline a practical way to solve equations (1)–(6), following Drittler *et al* [5]. First we factorize the cell potential in the form

$$V^n(\boldsymbol{r}) = U^n(\boldsymbol{r}) \Theta^n(\boldsymbol{r}), \tag{7}$$

where $\Theta^n(\boldsymbol{r})$ is a shape function, equal to 1 within the cell and zero otherwise, and $U^n(\boldsymbol{r})$ is a potential which extends smoothly beyond the cell boundary. $\Theta^n(\boldsymbol{r})$ and $U^n(\boldsymbol{r})$ are separately expanded in spherical harmonics, finally yielding a similar expansion for $V^n(\boldsymbol{r})$:

$$V^n(\boldsymbol{r}) = \sum_L V_L^n(r) Y_L(\hat{\boldsymbol{r}}). \tag{8}$$

The single-site wavefunctions $R_L^n(\boldsymbol{r}; E)$ and $H_L^n(\boldsymbol{r}; E)$ may also be expanded in spherical harmonics:

$$R_L^n(\boldsymbol{r}; E) = \sum_{L'} \frac{R_{L'L}^n(r; E)}{r} Y_{L'}(\hat{\boldsymbol{r}}) \tag{9}$$

$$H_L^n(\boldsymbol{r}; E) = \sum_{L'} \frac{H_{L'L}^n(r; E)}{r} Y_{L'}(\hat{\boldsymbol{r}}). \tag{10}$$

Substituting these expansions into the single-site Schrödinger equation yields coupled radial equations which $R_{L'L}(r; E)$ ($H_{L'L}(r; E)$) should satisfy for a given set of $V_L(r)$s. It is usually rather time-consuming to integrate these coupled differential equations. As an alternative, Drittler *et al* proposed solving perturbatively the integral equation

$$R_L^n(\boldsymbol{r}; E) = j_l(\sqrt{E}r) Y_L(\hat{\boldsymbol{r}}) + \int \mathrm{d}\boldsymbol{r}'\, g(\boldsymbol{r}, \boldsymbol{r}'; E) V^n(\boldsymbol{r}') R_L^n(\boldsymbol{r}'; E), \tag{11}$$

where $g(\boldsymbol{r}, \boldsymbol{r}'; E)$ is the free space Green function. Starting from the solution of the radial Schrödinger equation for the spherical part $V_{l=0,m=0}(r)$ of the potential, $R_l(r; E)$ and $H_l(r; E)$,

$R_{L'L}(r;E)$ ($H_{L'L}(r;E)$) can be calculated to an arbitrary order of the Born series by use of the recursive integral equation

$$R^{\rm out}_{LL'}(r;E) = R_l(r;E)\delta_{LL'} + \int_0^S r'^2 {\rm d}r'\, G_l(r,r';E) \sum_{L''} \Delta V_{LL''}(r') R^{\rm in}_{L''L'}(r';E) \tag{12}$$

$$H^{\rm out}_{LL'}(r;E) = H_l(r;E)\delta_{LL'} + \int_r^S r'^2 {\rm d}r'\, F_l(r,r';E) \sum_{L''} \Delta V_{LL''}(r') H^{\rm in}_{L''L'}(r';E), \tag{13}$$

where $G_l(r,r';E) = \sqrt{E} R_l(r_<;E) H_l(r_>;E)$ is the L diagonal single-site Green function for $V_{l=0,m=0}(r)$, and $\Delta V_{LL'}(r)$ is given by

$$\Delta V_{LL'}(r) = \sum_{L''(l''\neq 0)} C_{LL'L''} V_{L''}(r) \tag{14}$$

with $C_{LL'L''}$ being the Gaunt number in the usual notation. The superscripts 'in' and 'out' imply input and output for each iteration step. The differences between $R_{L'L}(r;E)$ and $H_{L'L}(r;E)$ are that for the latter $F_l(r,r';E) = \sqrt{E}[R_l(r;E)H_l(r';E) - R_l(r';E)H_l(r;E)]$ is used instead of $G_l(r,r';E)$ and the integration is performed from r to outside the potential range S. These differences come from the choice of the boundary condition. Since the non-spherical part of the potential is much smaller than the spherical part, we normally expect the iteration process to converge rapidly. Moreover, the procedure also yields the t-matrix of the cell potential (equation (6)). These features of the method will make the full potential KKR approach practicable.

The remaining part of the full potential KKR method is, except for the rather minor point that t-matrices are no longer diagonal, very much the same as the usual KKR method for the muffin-tin potentials, i.e., solving the Dyson-like equation (5).

In the full potential KKR method, it is important to get smooth convergence in the iteration procedure given by equations (12) and (13). Two important improvements for that are explained in the following subsections.

2.2. *Wronskian relation*

The Schrödinger equation with Green function $G_l(r,r';E)$ for the spherical part of the potential $V(r)$ is written as

$$\left[\frac{{\rm d}^2}{{\rm d}r^2} + E - \frac{l(l+1)}{r^2} + V(r)\right] G_l(r,r';E) = \delta(r-r'). \tag{15}$$

Through the radial integration, this equation shows that the derivative of $G_l(r,r';E)$ jumps at $r = r'$:

$$\lim_{\xi\to 0} \frac{{\rm d}G_l(r,r';E)}{{\rm d}r}\bigg|_{r=r'+\xi}^{r=r'-\xi} = 1. \tag{16}$$

Using $G_l(r,r';E) = \sqrt{E} R_l(r_<;E) H_l(r_>;E)$, the Wronskian between $R_l(r;E)$ and $H_l(r;E)$ is

$$W[R_l(r;E), H_l(r;E)] = R_l(r;E)H_l'(r;E) - R_l'(r;E)H_l(r;E) = \frac{1}{\sqrt{E}}, \tag{17}$$

where $R'(r) = {\rm d}R(r)/{\rm d}r$. This result is called the Wronskian relation. In order to obtain the correct Green function, we have to satisfy this relation with a very high precision. To this end, the regular and irregular solutions are numerically calculated by the following method. In the

numerical calculation, $R_l(r; E)$ is first determined starting from the origin and going towards the outside by solving the following equation for each l:

$$\begin{aligned} \frac{\mathrm{d}P(r)}{\mathrm{d}r} &= Q(r) \\ \frac{\mathrm{d}Q(r)}{\mathrm{d}r} &= \left[V(r) - E + \frac{l(l+1)}{r^2}\right] P(r), \end{aligned} \tag{18}$$

where $P(r)$ corresponds to $R_l(r; E)$. At the origin, $R_l(r; E)$ is set to r^{l+1} because

$$R_l(r; E) \propto r j_l(\sqrt{E}r) \sim r^{l+1} \qquad (r \to 0). \tag{19}$$

Then $H_l(r; E)$ is determined from the outside to the origin. At the boundary of the cell potential, $H_l(r; E)$ is set to the Hankel function, $h_l^{(1)}(z) = j_l(z) + \mathrm{i}n_l(z)$, where $n_l(z)$ is the Neumann function:

$$H_l(r; E) = -\mathrm{i}r h_l^{(1)}(\sqrt{E}r) \qquad r \geqslant S. \tag{20}$$

We show in the following that, in order for the Wronskian relation to be satisfied exactly, it is essential to use the fourth-order Runge–Kutta method. For the coupled differential equation,

$$x_i'(r) = f_i(\boldsymbol{x}, r), \tag{21}$$

the value x_i at the point $r + \Delta r$ is obtained from that at r in the fourth-order Runge–Kutta method as

$$x_i(r + \Delta r) = x_i(r) + \tfrac{1}{6}(k_{1i} + 2k_{2i} + 2k_{3i} + k_{4i}) + \mathrm{O}(\Delta r^5). \tag{22}$$

$$\begin{aligned} k_{1i} &= f_i(\boldsymbol{x}, r)\Delta r \\ k_{2i} &= f_i(\boldsymbol{x} + \tfrac{1}{2}\boldsymbol{k}_1, r + \tfrac{1}{2}\Delta r)\Delta r \\ k_{3i} &= f_i(\boldsymbol{x} + \tfrac{1}{2}\boldsymbol{k}_2, r + \tfrac{1}{2}\Delta r)\Delta r \\ k_{4i} &= f_i(\boldsymbol{x} + \boldsymbol{k}_3, r + \Delta r)\Delta r. \end{aligned}$$

Since the regular solution is solved from the origin towards the outside, $R(r + \Delta r)$ is obtained from that at the previous point r as

$$\begin{aligned} R(r + \Delta r) &= R(r) + \tfrac{1}{6}(k_{1P} + 2k_{2P} + 2k_{3P} + k_{4P}) \\ R'(r + \Delta r) &= R'(r) + \tfrac{1}{6}(k_{1Q} + 2k_{2Q} + 2k_{3Q} + k_{4Q}), \end{aligned} \tag{23}$$

$$\begin{aligned} k_{1P} &= R'(r)\Delta r & k_{1Q} &= F(r)R(r)\Delta r \\ k_{2P} &= (R'(r) + \tfrac{1}{2}k_{1Q})\Delta r & k_{2Q} &= F(r + \tfrac{1}{2}\Delta r)(R(r) + \tfrac{1}{2}k_{1P})\Delta r \\ k_{3P} &= (R'(r) + \tfrac{1}{2}k_{2Q})\Delta r & k_{3Q} &= F(r + \tfrac{1}{2}\Delta r)(R(r) + \tfrac{1}{2}k_{2P})\Delta r \\ k_{4P} &= (R'(r) + k_{3Q})\Delta r & k_{4Q} &= F(r + \Delta r)(R(r) + k_{3P})\Delta r \end{aligned}$$

where $F(r) = V(r) - E + \frac{l(l+1)}{r^2}$. It is found that $R(r + \Delta r)$ and $R'(r + \Delta r)$ can be written as linear combinations of $R(r)$ and $R'(r)$:

$$\begin{aligned} R(r + \Delta r) &= aR(r) + bR'(r) \\ R'(r + \Delta r) &= cR(r) + dR'(r). \end{aligned} \tag{24}$$

Now we assume that the Wronskian relation is satisfied for the regular and irregular solutions of equation (17) at the point $r + \Delta r$. With equation (24), the Wronskian at $r + \Delta r$ is written as

$$\begin{aligned} W[R(r + \Delta r), H(r + \Delta r)] &= aR(r)H'(r + \Delta r) + bR'(r)H'(r + \Delta r) \\ &\quad - cR(r)H(r + \Delta r) - dR'(r)H(r + \Delta r). \end{aligned} \tag{25}$$

Next, we consider the Wronskian at the previous point r. Since the irregular solution is solved from the outside towards the origin, $H(r)$ is obtained from that of the next point $r + \Delta r$ as

$$\begin{aligned} H(r) &= H(r+\Delta r) + \tfrac{1}{6}(\tilde{k}_{1P} + 2\tilde{k}_{2P} + 2\tilde{k}_{3P} + \tilde{k}_{4P}) \\ H'(r) &= H'(r+\Delta r) + \tfrac{1}{6}(\tilde{k}_{1Q} + 2\tilde{k}_{2Q} + 2\tilde{k}_{3Q} + \tilde{k}_{4Q}), \end{aligned} \tag{26}$$

$$\begin{aligned} \tilde{k}_{1P} &= -H'(r+\Delta r)\Delta r & \tilde{k}_{1Q} &= -F(r+\Delta r)H(r+\Delta r)\Delta r \\ \tilde{k}_{2P} &= -(H'(r+\Delta r) + \tfrac{1}{2}\tilde{k}_{1Q})\Delta r & \tilde{k}_{2Q} &= -F(r+\tfrac{1}{2}\Delta r)(H(r+\Delta r) + \tfrac{1}{2}\tilde{k}_{1P})\Delta r \\ \tilde{k}_{3P} &= -(H'(r+\Delta r) + \tfrac{1}{2}\tilde{k}_{2Q})\Delta r & \tilde{k}_{3Q} &= -F(r+\tfrac{1}{2}\Delta r)(H(r+\Delta r) + \tfrac{1}{2}\tilde{k}_{2P})\Delta r \\ \tilde{k}_{4P} &= -(H'(r+\Delta r) + \tilde{k}_{3Q})\Delta r & \tilde{k}_{4Q} &= -F(r)(H(r+\Delta r) + \tilde{k}_{3P})\Delta r \end{aligned}$$

and, then,

$$\begin{aligned} H(r) &= \tilde{a}H(r+\Delta r) + \tilde{b}H'(r+\Delta r) \\ H'(r) &= \tilde{c}H(r+\Delta r) + \tilde{d}H'(r+\Delta r). \end{aligned} \tag{27}$$

Hence the Wronskian at r is written as

$$\begin{aligned} W[R(r), H(r)] &= \tilde{c}R(r)H(r+\Delta r) + \tilde{d}R(r)H'(r+\Delta r) \\ &\quad - \tilde{a}R'(r)H(r+\Delta r) - \tilde{b}R'(r)H'(r+\Delta r). \end{aligned} \tag{28}$$

For the coupled differential equation which have the form of equation (18), $\{a, b, c, d\}$ and $\{a', b', c', d'\}$ have the following relation:

$$\begin{aligned} \tilde{a} &= d \\ \tilde{b} &= -b \\ \tilde{c} &= -c \\ \tilde{d} &= a. \end{aligned} \tag{29}$$

With this relation, the Wronskian at r is written as

$$\begin{aligned} W[R(r), H(r)] &= -cR(r)H(r+\Delta r) + aR(r)H'(r+\Delta r) \\ &\quad - dR'(r)H(r+\Delta r) + bR'(r)H'(r+\Delta r). \end{aligned} \tag{30}$$

This is nothing but the right-hand side of equation (25). Therefore,

$$W[R(r), H(r)] = W[R(r+\Delta r), H(r+\Delta r)]. \tag{31}$$

This means that, if the Wronskian relation is satisfied at the point $r+\Delta r$, the relation necessarily holds also at the point r. That is, the Wronskian relation is satisfied at all points irrespective of the step size $|\Delta r|$ as long as the relation is satisfied at the outermost point.

Equation (29) means that when we solve equation (18) from the origin towards the outside and then solve the same equation from the outside towards the origin, these two solutions are not equivalent unless $(ad - bc) = 1$. Now $(ad - bc) = 1 + \mathrm{O}(\Delta r^6)$, implying that there is numerical inaccuracy in the wavefunctions due to the use of the Runge–Kutta method. Nevertheless, relation (29) guarantees the Wronskian relation. The Wronskian relation comes from the singularity of the Green function, which is related to the number of states. We cannot count the number of states correctly unless the Green functions satisfy the Wronskian relation. In other words, we need the Wronskian relation to preserve the unitarity condition. Therefore the accuracy of the Wronskian relation is more important than that of wavefunctions themselves.

The Wronskians for potentials calculated with the fourth-order Runge–Kutta and Adams–Bashforth–Moulton methods are shown in figure 1. From the figure, it is clear that the Wronskian relation is obeyed with high precision by the Runge–Kutta method.

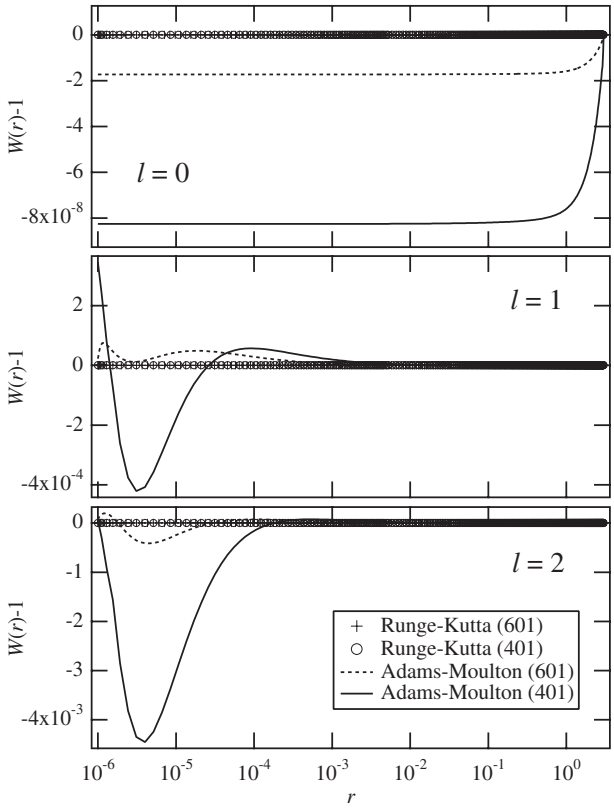

Figure 1. Wronskians for s, p and d states. They are calculated by the fourth-order Runge–Kutta and Adams–Bashforth–Moulton methods with 401 and 601 radial mesh points. Here the Wronskians are normalized to be 1, using the form $W(r) = (\sqrt{E})^{-1}[R_l(r; E)\{\mathrm{d}H_l(r; E)/\mathrm{d}r\} - \{\mathrm{d}R_l(r; E)/\mathrm{d}r\}H_l(r; E)]$. The solutions obtained by the Runge–Kutta method satisfy the Wronskian relation exactly up to a numerical precision of $\sim 10^{-16}$.

2.3. Recursive integral equation

In the recursive integral equation for the regular solution, equation (12), the integration is performed for the whole range. On the other hand, in the equation for the irregular solution, equation (13), the range of integration is from r to S. Equation (12) is a *Fredholm equation* while equation (13) is a *Volterra equation*. In the Fredholm equation, the wavefunction does not converge when, for instance, $\Delta V_{LL'}(r)$ is large, or the energy is near a resonance, and so on. In the Volterra equation, the wavefunction certainly converges even in the above cases, because the solution is fixed at the edge point of the integration range [8]. In order to obtain the regular solution, we should employ an alternative scheme to obtain convergence.

In equation (12), the regular solution $R_{LL'}(r; E)$ is expressed as

$$R^{\mathrm{out}}_{LL'}(r; E) = R_l(r; E)\delta_{LL'} + \int_0^S r'^2 \mathrm{d}r'\, G_l(r, r'; E) \sum_{L''} \Delta V_{LL''}(r') R^{\mathrm{in}}_{L''L'}(r'; E). \tag{32}$$

It can be rewritten in the following way:

$$R^{\mathrm{out}}_{L'L}(r; E) = R_l(r; E)\gamma_{LL'}(E) - \int_0^r r'^2 \mathrm{d}r' F_{l'}(r, r'; E) \sum_{L''} \Delta V_{L'L''}(r') R^{\mathrm{in}}_{L''L'}(r'; E), \tag{33}$$

where

$$\gamma_{LL'}(E) = \delta_{LL'} + \frac{1}{\sqrt{E}} \int_0^S \mathrm{d}r' H_l(r'; E) \sum_{L''} \Delta V_{LL''}(r') R_{L''L'}(r'; E). \tag{34}$$

Here, $\gamma_{LL'}(E)$ is independent of r and can be treated as a constant. Then the new function $P_{LL'}(r; E)$ is introduced:

$$P_{LL'}(r; E) = \sum_{L''} R_{LL''}(r; E) \gamma^{-1}_{L''L'}(E). \tag{35}$$

Hence equation (33) becomes

$$P^{\mathrm{out}}_{L'L}(r; E) = R_l(r; E)\delta_{LL'} - \int_0^r r'^2 \mathrm{d}r' F_{l'}(r, r'; E) \sum_{L''} \Delta V_{L'L''}(r') P^{\mathrm{in}}_{L''L'}(r'; E). \tag{36}$$

Now the equation is a Volterra equation and hence always converges. The normalization $\gamma_{LL'}(E)$ can be obtained from the boundary condition.

Examples of the densities of states (DOSs) calculated with the Fredholm and Volterra equations are shown in figure 2. One can see that the Fredholm equation obviously fails: the DOS at the bound state oscillates between positive and negative values and never converges. On the other hand, the result obtained from the Volterra equation converges after a few iterations.

With these improvements, the full potential KKR method becomes a very stable and accurate method for electronic structure calculation for arbitrary solids. Since the computational time is much shorter than for the FLAPW method, our method can be used for calculations for complex systems.

2.4. Modified single-site Green function

In order to construct charge/spin densities, we have to perform an energy integration of the imaginary part of the Green function $\mathrm{Im}\, G(\boldsymbol{r}, \boldsymbol{r}; E)$. In the KKR Green function method, this is performed along an integration path deformed into the upper complex half-plane so as to overcome the difficulty in performing the numerical integration near resonances and bound states. This, however, causes another problem: normally, the single-site Green function contains irregular solutions (equation (2)). Such solutions do not contribute to charge/spin densities and can be subtracted beforehand for real energies as is explained below. Unfortunately, this is not possible along the complex integration path. This means that the elimination of the contribution of the irregular solutions has to be done numerically. This often causes problems in the charge/spin densities in the vicinity of the nucleus. It is clear that the singular behaviour of the irregular solutions near the origin cannot be completely cancelled out with numerical complex energy integration. This is particularly serious for the calculation of EFGs.

As mentioned above, as long as the integration is performed along the real axis, only the regular solutions are needed. This can be seen from the following consideration: let us divide the irregular solution $H^n_L(\boldsymbol{r})$ of the single-site Schrödinger equation into a purely irregular part $N^n_L(\boldsymbol{r})$ and a regular part as

$$H^n_L(\boldsymbol{r}; E) = N^n_L(\boldsymbol{r}; E) + \xi^n_L(E) R^n_L(\boldsymbol{r}; E), \tag{37}$$

where $\xi^n_L(E)$ does not depend on $\boldsymbol{r}$. Since the Hamiltonian is real, both $N^n_L(\boldsymbol{r})$ and $R^n_L(\boldsymbol{r})$ are real apart from some complex factors. Combining this fact with a Wronskian relation between $R^n_L(\boldsymbol{r})$ and $H^n_L(\boldsymbol{r})$ (or, equivalently, that between $R^n_L(\boldsymbol{r})$ and $N^n_L(\boldsymbol{r})$), we can show that $\sqrt{E} R^n_L(\boldsymbol{r}; E) N^n_L(\boldsymbol{r}; E)$ is always real. From the above, together with the fact that

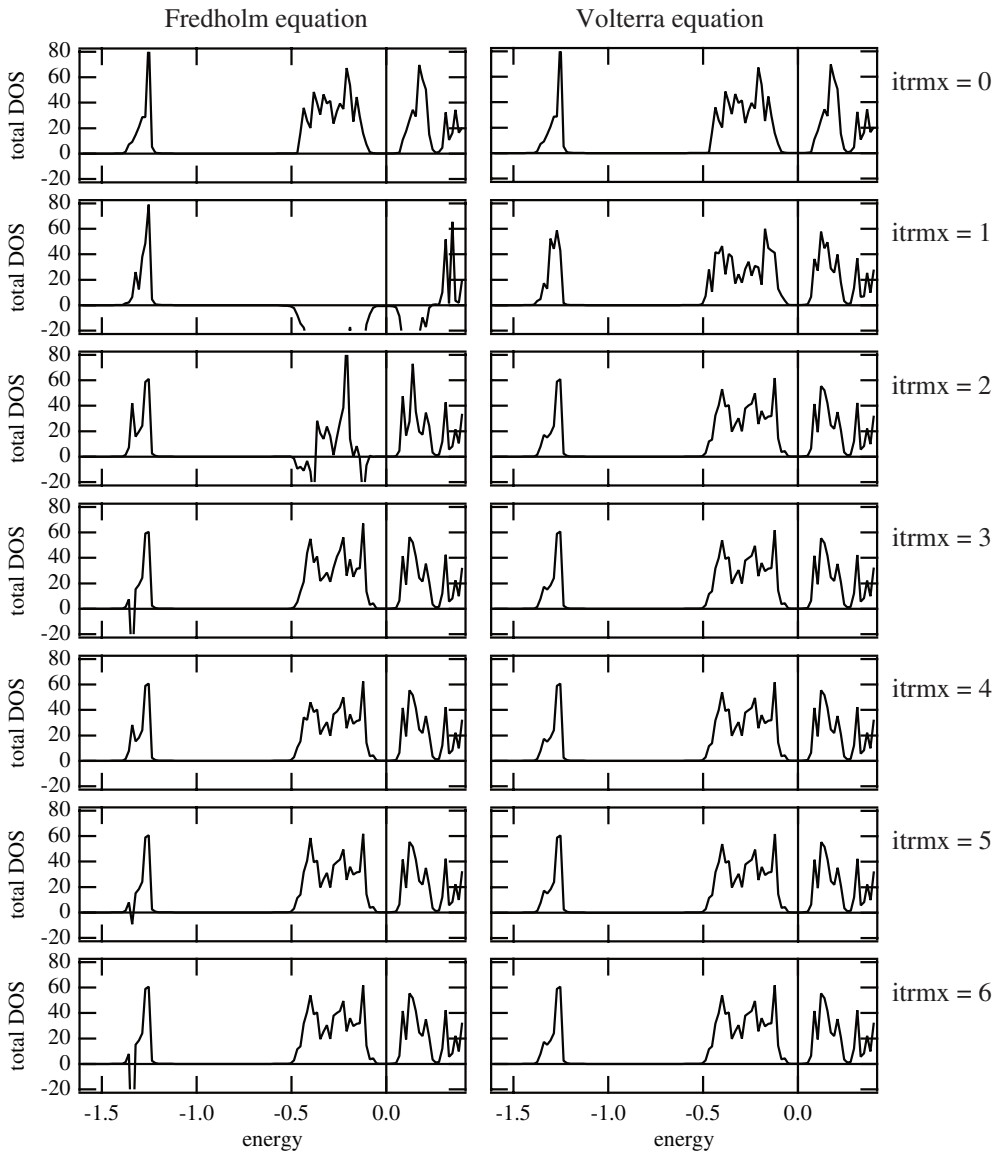

Figure 2. Total DOS of TiO_2, calculated using the Fredholm and Volterra equations. The parameter 'itrmx' means the order of the Born series.

$\{R_L^n(\boldsymbol{r};E)\}^2/\int_\Omega \mathrm{d}\boldsymbol{r}\,\{R_L^n(\boldsymbol{r};E)\}^2$ is also real for a real Hamiltonian, we conclude that

$$\mathrm{Im}\,\sqrt{E}R_L^n(\boldsymbol{r};E)H_L^n(\boldsymbol{r};E) = \mathrm{Im}\,\sqrt{E}\left\{R_L^n(\boldsymbol{r};E)\right\}^2\frac{\int_\Omega \mathrm{d}\boldsymbol{r}\,R_L^n(\boldsymbol{r};E)H_L^n(\boldsymbol{r};E)}{\int_\Omega \mathrm{d}\boldsymbol{r}\{R_L^n(\boldsymbol{r};E)\}^2} \tag{38}$$

must be satisfied for real energy E. Here, the region of the volume integration Ω is arbitrary. This means that, as far as the imaginary part of $G_s^n(\boldsymbol{r},\boldsymbol{r};E)=\sum_L\sqrt{E}R_L^n(\boldsymbol{r};E)H_L^n(\boldsymbol{r};E)$ on the real axis is concerned, we may replace the single-site Green function with the modified

Green function

$$\tilde{G}_s^n(\boldsymbol{r}, \boldsymbol{r}; E) = \sum_L \sqrt{E} \left\{ R_L^n(\boldsymbol{r}; E) \right\}^2 \frac{\int_\Omega \mathrm{d}\boldsymbol{r}\, R_L^n(\boldsymbol{r}; E) H_L^n(\boldsymbol{r}; E)}{\int_\Omega \mathrm{d}\boldsymbol{r}\, \{R_L^n(\boldsymbol{r}; E)\}^2}. \tag{39}$$

It is shown that the true single-site Green function and its replacement have the same analytic properties, i.e., they are both analytic in the upper complex half-plane (see the discussion in [9]). This contrasts sharply with the fact that $\sum_L \sqrt{E}\xi_L^n(E)\{R_L^n(\boldsymbol{r}; E)\}^2$ does not have this property. For this reason, it cannot be used in place of the true single-site Green function when the analytic property of the Green function is important. In our observation, the use of the modified single-site Green function $\tilde{G}_s^n(\boldsymbol{r}, \boldsymbol{r}; E)$ is crucial for the calculation of EFGs. It also improves the quality of the self-consistent potential and thus ensures the accuracy of the full potential KKR. Yet another method that eliminates irregular solutions was proposed for the muffin-tin KKR method [9]. The method unfortunately cannot be applied directly in the present case of a full potential KKR approach.

3. EFG calculation

The electric field gradient tensor is defined in terms of the second derivatives of the Coulomb potential at the nucleus in Cartesian coordinates:

$$V_{ij} = \left. \frac{\partial^2 V(\boldsymbol{r})}{\partial r_i \partial r_j} \right|_{r=0} \qquad (i, j = x, y, z). \tag{40}$$

$V(\boldsymbol{r})$ is produced by the electron density distribution $\rho(\boldsymbol{r})$. In the full potential KKR method, the electron density is expanded in spherical harmonics, which is convenient for the EFG calculation. For EFG, only $l = 2$ components remain:

$$\left. \frac{\partial^2 V(\boldsymbol{r})}{\partial r_i \partial r_j} \right|_{r=0} = \sum_m \sqrt{\frac{4\pi}{5}} V_2^m \frac{\partial^2}{\partial r_i \partial r_j} r^2 Y_{2,m}(\hat{\boldsymbol{r}}), \tag{41}$$

where

$$V_l^m = \sqrt{\frac{4\pi}{2l+1}} \int \mathrm{d}\boldsymbol{r}\, \frac{\rho(\boldsymbol{r})}{r^{l+1}} Y_L^*(\hat{\boldsymbol{r}}). \tag{42}$$

3.1. hcp metals

The hcp structure is one of the simplest structures of elements which has a non-vanishing EFG. Considering the crystal symmetry we can set the asymmetry parameter η to be zero. The EFGs of hcp metals have been studied extensively both experimentally and theoretically. In this regard, these systems are suitable for examining the reliability of the present procedure for the EFG calculation.

The EFG calculation was performed for Be, Mg, Sc, Ti, Co, Zn, Y, Zr, Tc, Ru, Cd, La, Hf, Re, Os and Tl. Most of these are transition metals. The wavefunctions were expanded in real harmonics up to $l = 2$, the potential and the charge density up to $l = 4$ and the shape functions up to $l = 8$. We checked the convergence with respect to the angular momentum l cut-off and it was found that the influence of the l cut-off is very small for EFG calculations. For the KKR matrix, summation of 3234 k-points in the irreducible wedge of the first Brillouin zone were used. The exchange–correlation potential was calculated with the parameters in [10]. The lattice constants [11] are summarized in table 1. The calculation was performed both in the non-relativistic and scalar relativistic approximations [12, 13].

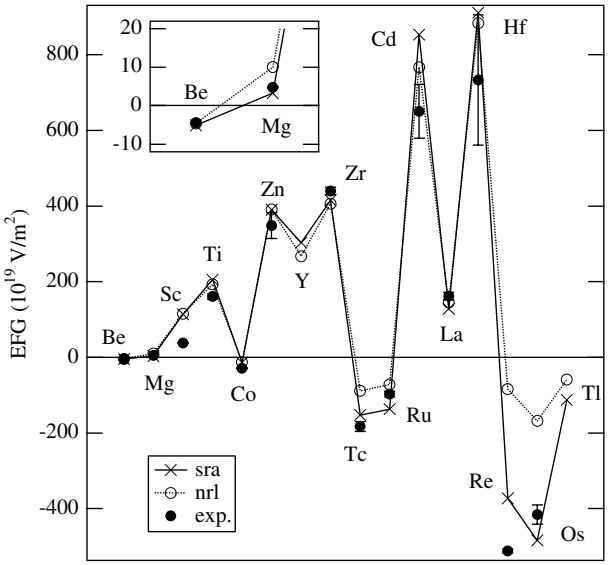

Figure 3. Theoretical and experimental EFGs in HCP metals.

The results are shown in table 1 and figure 3. In the table, experimental data [14] and the theoretical results obtained by the FLAPW calculation [16] are also listed. EFGs of hcp metals show the following systematic behaviour:

(1) At the beginning of the d series, EFGs are positive and increase as the number of d electrons increases.

(2) At the centre of the d series, EFGs are negative and decrease in absolute value as the number of d electrons increases.

(3) At the end of the d series, EFGs turn to positive large values.

(4) The variation in EFGs through the d series is more prominent for the higher periods.

This trend is the same as that pointed out by Blaha *et al* [16]. The dominant contribution to the EFG is that of the p orbitals. The larger occupation of p_x and p_y compared with p_z leads to a positive EFG and vice versa. In the present cases, the DOSs of p_x and p_y components have larger amplitude at lower energy region while that of p_z is dominant at higher energies. Therefore, the simple band filling effect leads to the systematic change of the EFGs [16]. Our calculation reproduces this trend and shows good agreement with the experimental values. The present results are not very different from those from the FLAPW method for Be–Cd. For La–Tl, for which no results calculated by the FLAPW method are available, the same trend is confirmed.

Tc, Ru, Re and Os are located at the centre of the d series and have large atomic numbers. For such elements, the relativistic effect is large and the difference between non-relativistic and scalar relativistic calculations is remarkable. For more detailed discussions, full relativistic treatments that take account of the extra EFG induced by the spin–orbit coupling may be necessary [17].

Table 1. Lattice constants of hcp metals in Å [11] and theoretical and experimental EFGs in hcp metals [14–16] in units of 10^{19} V m^{-2}. All experimental EFGs are recalculated using the most recent reference values for the nuclear quadrupole moments [18, 19]. Values written without signs indicate that their signs are not determined. 'nrl' and 'sra' mean the non-relativistic and scalar relativistic approximations, respectively.

			This work			
Element	a	c	nrl	sra	FLAPW	Exp.
Be	2.286 6	3.583 3	−4.6	−5.1	−4.2	4.42 ± 0.04
Mg	3.209 27	5.210 33	+10	+3.3	+4.8	4.8 ± 0.24
Sc	3.309 0	5.273 3	+114	+114	+96	38.0 ± 0.7
Ti	2.950	4.686	+193	+205	+207	161 ± 7
Co	2.507 1	4.068 6	−13	−14	−19	−29 ± 1
Zn	2.664 8	4.946 7	+391	+390	+375	+348 ± 34
Y	3.647 4	5.730 6	+267	+303	+279	—
Zr	3.232	5.147	+406	+415	+429	440 ± 10
Tc	2.743	4.400	−89	−153	−147	183 ± 13
Ru	2.703 89	4.281 68	−72	−137	−123	97 ± 7
Cd	2.978 87	5.617 65	+767	+853	+762	+650 ± 71
La	3.75	6.07	+145	+128	—	162 ± 10
Hf	3.196 7	5.057 8	+883	+911	—	+733 ± 172
Re	2.760 8	4.458 2	−84	−373	—	−512 ± 5
Os	2.735 2	4.319 0	−168	−484	—	−416 ± 25
Tl	3.456	5.525	−59	−113	—	—

3.2. Impurities in Zn and Cd

The behaviours of the EFGs in hcp metals in the previous subsection are explained by the band filling effect. However, it is also possible that the c/a ratio, which varies from element to element, might also affect EFGs. In this respect, clearer evidence of a systematic variation may be seen in the case of EFGs of impurities in a common host. For this reason, we tried the full potential KKR calculation on impurity systems. Another reason that we perform such a calculation is that there are a lot of experimental EFG data for impurities in non-cubic systems. In order to discuss such EFGs, we need to be able to deal with the impurity systems in the same way as pure systems and to check the reliability for the impurity calculation. Here we show the EFG calculations for 4sp (Cu–Kr) and 5sp (Ag–Xe) impurities in Zn and Cd. We assume, as an empirical rule for heavy impurities, that the impurity atoms sit at the substitutional site in the hcp crystals of Zn and Cd.

The EFGs of those impurities show systematic trends and they have been studied theoretically [20–23]. As shown in the previous subsection, the EFG is mainly created by the non-spherical p charge. In analysing the contribution of the p charge to the EFGs, it is important to notice that Zn and Cd have c/a ratios of 1.856 and 1.886, respectively. They are much larger than the ideal ratio of hcp structure, 1.633. The p_x and p_y orbitals have a stronger overlap than the p_z orbitals because of the large c/a ratio. This leads to a broader density of states of p_x and p_y than p_z. Near the top of the p band, though the p_x and p_y components at the Fermi level are larger than the p_z components, the p_z components are still in the majority in the integrated density of states. One finds that the EFG shows an *S*-shape behaviour, being positive for a less than half-filled band, vanishing for the half-filled band and being negative for higher band fillings [2, 20–23].

The procedure of calculation is similar to that used for hcp metals in the previous subsection. The supercell method was employed to simulate the impurity system. We defined

Table 2. Theoretical and experimental EFGs of sp impurities in Zn and Cd [14] in units of 10^{19} V m^{-2}. All experimental EFGs are recalculated using the most recent reference values for the nuclear quadrupole moments [18, 19]. Values written without signs indicate that their signs are not determined.

	Zn host		Cd host	
Impurity	Theor.	Exp.	Theor.	Exp.
Cu	+170	—	+90	—
Zn	+390	+348 ± 34	+315	272 ± 27
Ga	+576	514 ± 41	+463	440 ± 31
Ge	+532	301 ± 69	+418	179 ± 41
As	−193	—	−599	—
Se	−1618	—	−1519	—
Br	−1431	860 ± 220	−766	690 ± 173
Kr	−660	817 ± 32	−232	396 ± 27
Ag	+864	+193 ± 15	+575	420 ± 50
Cd	+1284	+685 ± 61	+853	+650 ± 71
In	+1457	+1256 ± 22	+963	+1002 ± 16
Sn	+1433	+1186 ± 68	+976	+820 ± 10
Sb	+474	—	−326	35 ± 4
Te	−1374	—	−2361	—
I	−3314	−2200 ± 700	−2299	−1700 ± 170
Xe	−2636	—	−999	360 ± 38

the supercell so that it consists of six primitive unit cells of the hcp structure and one of the host atoms was replaced by the impurity. The calculation was performed with the scalar relativistic approximation. 270 k-points in the irreducible wedge of the first Brillouin zone were used. The local lattice relaxation around the impurity was taken into account for nearest neighbour atoms. Here the lattice relaxation was determined from the total energy of the system assuming that the relaxation is isotropic. For more general relaxations, we should introduce the force calculation [24] in addition to the total energy calculation.

The results are shown in table 2 and figure 4 together with the experimental data [14]. In the figure, the results of the KKR calculation with the muffin-tin potential model are also shown. The overall trends for the experimental EFGs are well reproduced by the theoretical predictions. The agreement is obviously improved with the full potential treatment. Though the impurity concentration in the present calculation is rather higher than in the experimental situations, the results show good agreements and the size of the supercell seems large enough. Even for such a large supercell the cpu time is reasonable and the present method will be useful for EFG calculations for various impurity systems.

4. Conclusion

We developed a full potential KKR Green function method. The following improvements make the full potential method stable and accurate. Using the fourth-order Runge–Kutta method, we can obtain wavefunctions which satisfy the Wronskian relation exactly. Such wavefunctions give correct Green functions. The recursive integral equations which involve the non-spherical part of the potential were modified from the Fredholm type to the Volterra type. With the correct Green function and the modified integral equations, the non-spherical part of the potential is taken into account for wavefunctions exactly. Thirdly, using a modified single-site Green function instead of the true one completely eliminates the singular contribution of the irregular

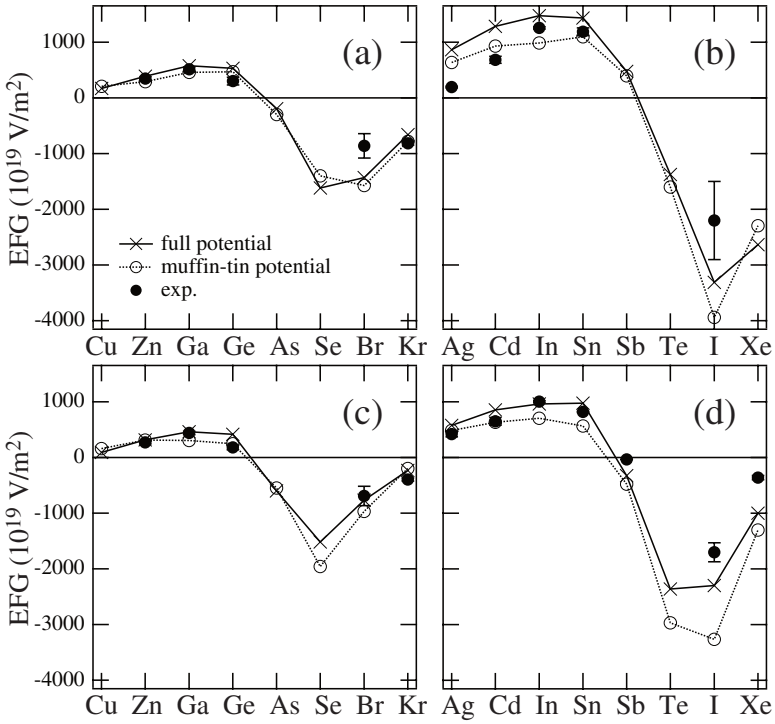

Figure 4. Theoretical and experimental EFGs of 4sp impurities in Zn (a), 5sp impurities in Zn (b), 4sp impurities in Cd (c) and 5sp impurities in Cd (d).

solutions of the Schrödinger equation to the charge/spin densities. This greatly improves the quality of numerical calculations.

By use of the full potential KKR method, the EFGs of hcp metals and impurities in Zn and Cd are calculated. It is demonstrated that the full potential KKR method is effective for the EFG calculation not only for pure systems but also for impurity systems. The EFG calculation can be performed not only for metals reported in this paper but also for ionic substances [25]. Calculation by this method is faster and more compact than the FLAPW calculation and hence more complex systems can be treated. Taking account of that, the full potential KKR method is one of the best practical methods for EFG calculation.

Besides EFG calculations, full potential treatment shows potential for any calculations which are affected by the anisotropy of the charge distribution, such as ones for orbital ordering, surface and interface effects, molecules and clusters. Test calculations for these complex systems are desirable.

Acknowledgments

We acknowledge Dr K Sato, The Institute of Scientific and Industrial Research, Osaka University, and Drs P H Dederichs and R Zeller, Forschungszentrum Jülich, for fruitful discussions. The present study was partly supported by the 21st century COE programme 'Towards a New Basic Science', by Special Coordination Funds for the Promotion of Science and Technology, Leading Research 'Nanospintronics Design and Realization', by Research and Development for Applying Advanced Computational Science and Technology 'Development

of Computational Nano-Material Design', Japan Science and Technology Agency, and by the Nano Technology Programme, New Energy and Industrial Technology Development Organization, Japan.

References

[1] Schwarz K and Blaha P 1996 *Lecture Notes Chem.* **67** 139
[2] Akai H, Akai M, Blügel S, Drittler B, Ebert H, Terakura K, Zeller R and Dederichs P H 1990 *Prog. Theor. Phys. Suppl.* **101** 11
[3] Akai H 1982 *J. Phys. Soc. Japan* **51** 468
[4] Drittler B, Weinert M, Zeller R and Dederichs P H 1990 *Phys. Rev.* B **42** 9336
[5] Drittler B, Weinert M, Zeller R and Dederichs P H 1991 *Solid State Commun.* **79** 31
[6] Zeller R 1987 *J. Phys. C: Solid State Phys.* **20** 2347
[7] Williams A R, Janak J F and Moruzzi V L 1972 *Phys. Rev.* B **6** 4509
[8] Newton R G 1960 *J. Math. Phys.* **1** 319
[9] Kotani T and Akai H 1996 *Phys. Rev.* B **54** 16502
[10] Moruzzi V L, Janak J F and Williams A R 1978 *Calculated Electronic Properties of Metals* (Oxford: Pergamon)
[11] Wyckoff R W G 1963 *Crystal Structures* 2nd edn (New York: Interscience)
[12] Koelling D D and Harmon B N 1977 *J. Phys. C: Solid State Phys.* **10** 3107
[13] Takeda T 1978 *Z. Phys.* B **32** 43
[14] Vianden R 1983 *Hyperfine Interact.* **15/16** 1081
[15] Ebert H, Abart J and Voitländer J 1986 *J. Phys. F: Met. Phys.* **16** 1287
[16] Blaha P, Schwarz K and Dederichs P H 1988 *Phys. Rev.* B **37** 2792
[17] Huhne T, Zecha C, Ebert H, Dederichs P H and Zeller R 1988 *Phys. Rev.* B **58** 10236
[18] Pyykkö P 2001 *Mol. Phys.* **99** 1617
[19] Raghavan P 1989 *At. Data Nucl. Data Tables* **42** 189
[20] Haas H, Menningen M, Andreasen H, Damgaard S, Grann H, Petersen F T, Petersen J W, Weyer G (ISOLDE Collaboration) 1983 *Hyperfine Interact.* **15/16** 215
[21] Haas H 1986 *Z. Naturf.* a **41** 78
[22] Lindgren B 1986 *Phys. Rev.* B **34** 648
[23] Schmidt P C, Weiss Al, Cabus S and Kübler J 1988 *Z. Naturf.* a **42** 1321
[24] Papanikolaou N, Zeller R, Dederichs P H and Stefanou N 1997 *Phys. Rev.* B **55** 4157
[25] Ogura M and Akai H 2005 *Hyperfine Interact.* at press